Bulletin of the Seismological Society of America, Vol. 96, No. 1, pp. 133–146, February 2006, doi: 10.1785/0120030243

3D Ground-Motion Estimation in Rome, Italy

by K. B. Olsen, A. Akinci, A. Rovelli, F. Marra, and L. Malagnini

Abstract Paleoseismic evidence and seismic-hazard analysis suggest that the city of Rome, Italy, has experienced considerable earthquake ground motion since its establishment more than 2000 years ago. Seismic hazards in Rome are mainly associated with two active seismogenic areas: the Alban Hills and the Central Apennines regions, located about 20 km southeast and 80–100 km east of central Rome. Within the twentieth century, *M* 6.8 and *M* 5.3 earthquakes in the Apennines and the Alban Hills, respectively, have generated intensities up to Mercalli-Cancani-Sieberg scale (MCS) VII in the city. With a lack of strong-motion records, we have generated a 3D velocity model for Rome, embedded in a 1D regional model, and estimated long-period (<1 Hz) ground motions for such scenarios from finite-difference simulations of viscoelastic wave propagation. We find 1-Hz peak ground velocities (PGVs) and peak ground accelerations (PGAs) of up to 14 cm/sec and 44 cm/sec^2, respectively, for a *M* 5.3 Alban Hills scenario, largest near the northwestern edge of the Tiber River. Our six simulations of a *M* 7.0 Central Apennine scenario generate 0.5-Hz PGVs in Rome of up to 9 cm/sec, as well as extended duration up to 60 sec. The peak motions are similar to, but the durations much longer than those from previous studies that omitted important wave-guide effects between the source and the city. The results from the two scenarios show that the strongest ground-motion amplification in Rome occurs in the Holocene alluvial areas, with strong basin edge effects in the Tiber River valley. Our results are in agreement with earlier 2D *SH*-wave results showing amplification of peak velocities by up to a factor of 2 in the alluvial sediments, largest near the contact to the surrounding Plio-Pleistocene formations. Our results suggest that both earthquakes from the Alban Hills and the Central Apennines regions contribute to the seismic hazards in Rome. Although earthquakes from the former area may generate the larger peak motions, seismic waves from the latter region may generate ground motions with extended durations capable of causing significant damage on the built environment.

Introduction

The Italian earthquake catalog, spanning more than 2000 years, includes several earthquakes that were felt in Rome and produced significant damage even to Imperial Age monuments (first to fifth century). The first written reports in the catalog are from 82 B.C.; since that time the city has suffered approximately 20 events of widespread damage, in some cases, severe (Molin *et al.*, 1995; Donati *et al.*, 1999). Regional seismicity, represented by Central Apennine seismogenic sources located about 100 km from Rome (see Fig. 1) has produced the strongest Mercalli-Cancani-Sieberg scale (MCS) intensities (Sieberg, 1930) in the city (VII–VIII MCS for the 1349, 1703, and 1915 earthquake sequences; see Table 1). Paleoseismic studies show that the magnitude of these earthquakes might have been 7.0 or larger (Pantosti *et al.*, 1996). Local seismicity (see Fig. 1) is associated mainly with the Alban Hills volcanic district, characterized by frequent earthquakes felt in the city with approximate intensities of V–VI MCS, maximum magnitudes of about 5 (Amato *et al.*, 1994), and hypocentral depths between 5 and 10 km. The earthquake of 19 July 1899 was the most recent event generated in this seismogenic district to cause damage in Rome (up to VI MCS). The Alban Hills area was investigated in detail by Amato *et al.* (1994) and Chiarabba *et al.* (1994) with respect to both the recurrence and magnitude pattern of the local seismicity. A comprehensive revision of the historical sources concerning the earthquakes felt in Rome was performed by Molin and Guidoboni (1989) (see summary in Table 1).

Strong-motion data collected for recent large earthquakes around the world using dense arrays have shown extreme diversification of the damage within urban areas. Analysis of these data also shows that the near-surface ge-

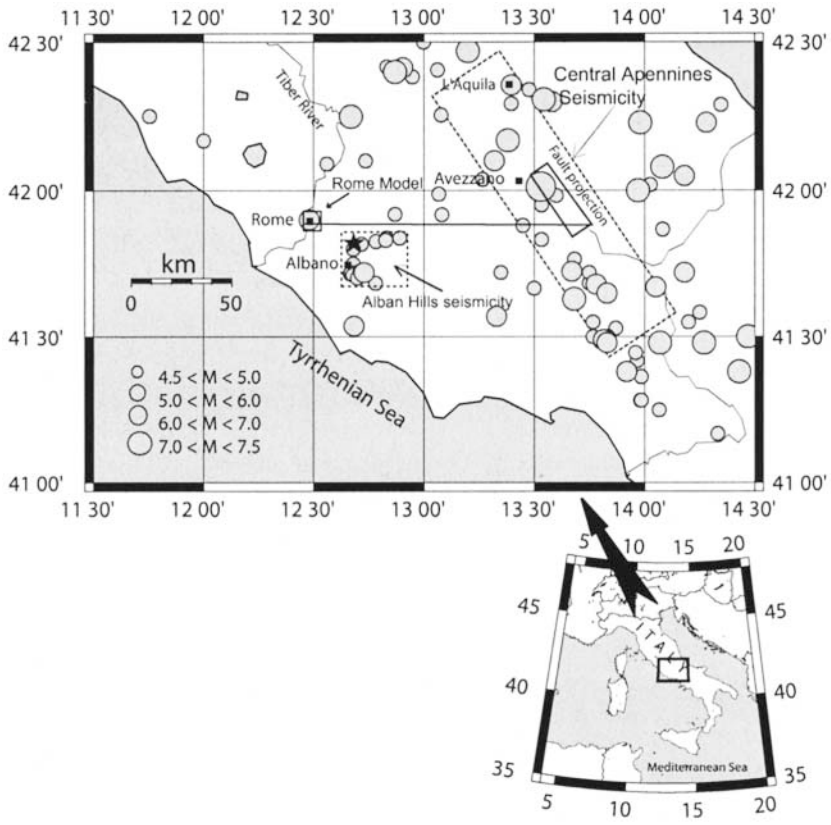

Figure 1. The seismicity near Rome estimated from earthquakes of the Italian catalog, Catalogo Parametrico dei Terremoti Italiani (Gruppo di Lavoro, CPTI, 1999). Dotted rectangles present the two main seismogenic districts affecting the city (the Central Apennines and the Alban Hills). We simulate ground motions produced in the city by two scenario earthquake locations: (1) the Alban Hills, at an average distance of 25 km from Rome and (2) the Central Apennines located 80–100 km from Rome. The filled star shows the epicenter location of the M 5.3 Alban Hills scenario earthquake. Solid rectangles depict the Rome model and the fault projection that is used for the Central Apennines scenario earthquake, taken from the database of Valensise and Pantosti, (2001) for the 13 January 1915 Fucino earthquake, M 7.0. The horizontal line depicts the profile used to display synthetic seismograms for the Fucino earthquake scenario in Figure 9.

Table 1
Major Local and Regional Earthquakes Felt in Rome
(Molin and Guidoboni, 1989)

Data	I_0	I_R	Origin Area
83 B.C.	—	—	Unknown
72–70 B.C.	—	—	Unknown
51	—	—	Unknown
443	—	—	Unknown
484 or 508	—	—	Unknown
801	—	VII–VIII	Central Apennines
1349	X	VII–VIII	L'Aquila
1703	X	VII	L'Aquila
1812	VII	VII	Rome
1899	VII–VIII	VI	Albani Hills
1915	XI	VI–VII	Fucino

I_0 = epicentral MCS intensity; I_R = MCS intensity estimated in Rome.

ology can amplify the incident waves considerably to produce ground motion causing severe damage locally. For example, such amplified ground motion caused a large part of the damage that occurred in Mexico City during the 19 September 1985, M_s 8.1 earthquake (Singh *et al.*, 1988), the 1988 M_s 6.8 Armenian earthquake (Hadjian, 1993), the 1989 M_s 7.1 Loma Prieta earthquake (Seekings and Boatwright, 1994), and the 1995 M_s 6.9 Kobe earthquake (Kawase, 1996; Pitarka *et al.*, 1996; Motosaka and Nagano, 1997). Although Rome was settled in a relatively low-seismicity area, it may yet suffer earthquake damage, in particular, in its historical center, where shallow geological heterogeneities and large deposits of recent, unconsolidated sediments overlying Pliocene bedrock may cause significant amplification effects (Salvi *et al.*, 1991). For example, Rovelli *et al.* (1994, 1995) showed, by using 2D finite-difference simulations, that large ground-motion amplification tends to occur at the boundaries of the valley because of topographic irregularities and edge effects at the sharp Pliocene-Holocene discontinuity. Fäh *et al.* (1993, 1995) used a hybrid technique based on mode summation and finite differences to simulate 2-Hz ground motion in Rome for the 13 January 1915 Fucino earthquake. They found peak accelerations of up to 60 cm/sec^2 and maximum amplification factors of 5–6 within their 2D basin model of Rome with respect to a 1D model, caused by resonance effects and the excitation of local surface waves. The largest amplification was observed at the edge of the sedimentary basin of the Tiber River valley (87 km from the source), and they showed good correlation between the ground motions and the observed distribution of damage in Rome. Figure 2 shows the distribution of building damage that occurred in the urban area from the Fucino earthquake, indicating a strong correlation with the presence of the underlying alluvium. Finally, recent studies of the seismic response of Rome (Iodice *et al.*, 1992; Boschi *et al.*, 1995; Funiciello *et al.*, 1995) show large amplification effects on the soft Holocene deposits of the Tiber river from modeling of ground motion produced by the 1915 Avezzano earthquake.

Unfortunately, none of the local or regional events dis-

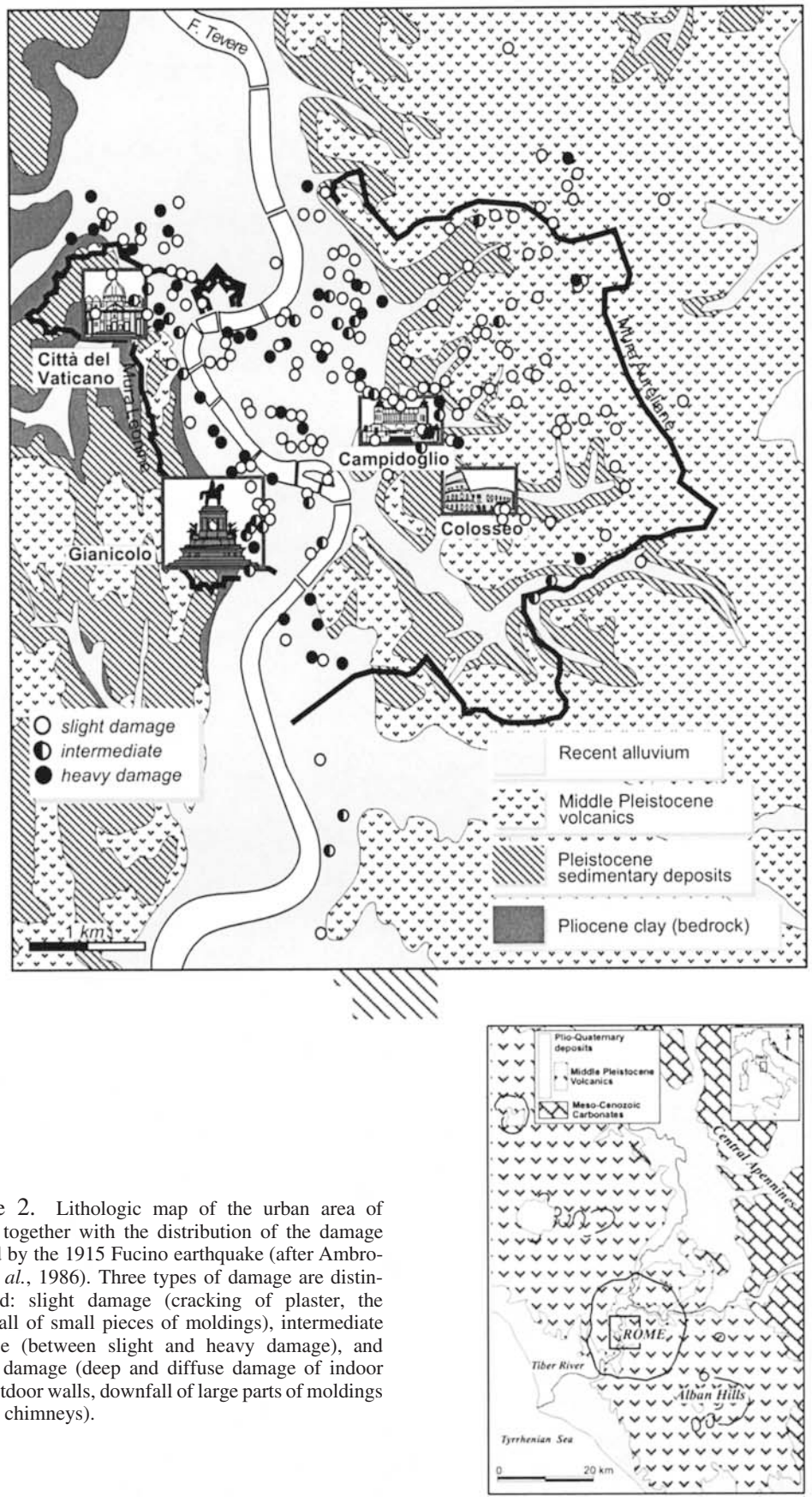

Figure 2. Lithologic map of the urban area of Rome together with the distribution of the damage caused by the 1915 Fucino earthquake (after Ambrosini *et al.*, 1986). Three types of damage are distinguished: slight damage (cracking of plaster, the downfall of small pieces of moldings), intermediate damage (between slight and heavy damage), and heavy damage (deep and diffuse damage of indoor and outdoor walls, downfall of large parts of moldings and of chimneys).

cussed previously were recorded by seismic stations within Rome. However, the recent appearance of more powerful computers, better constrained basin models, and more efficient numerical wave propagation codes have facilitated computation of the 3D long-period seismic response of numerous sedimentary basins throughout the world (e.g., Frankel and Vidale, 1992; Yomogida and Etgen, 1993; Olsen and Schuster, 1995; Olsen *et al.*, 1995; Olsen and Archuleta, 1996; Graves, 1996; Wald and Graves, 1998; Olsen, 2000; Olsen *et al.*, 2003). In this study, we present a new 3D subsurface model of Rome that is constrained by more than 1000 borehole measurements. We use the model to compute ground motions for the Central Apennine and Alban Hills scenarios.

This article is organized as follows. First, we describe the subsurface model of Rome, the numerical modeling approach, and the seismic sources included in our study. Then we describe the numerical results by using snapshots of the simulated wave-field and synthetic seismograms. Finally, we discuss our results in relation to previous ground-motion estimates for Rome.

Subsurface Model of Rome

The local geology of the Rome area consists of shallow, continuous bedrock made of consolidated Pliocene clays covered by less-consolidated Pleistocene sedimentary pyroclastic rocks and Holocene deposits (Fig. 2). Below a depth of approximately 1 km the Plio-Pleistocene clay is replaced by a carbonatic substrate, Meso-Cenozoic in age. The historical center of the city is characterized by the presence of a complex drainage network filled with recent alluvial deposits and subsequently hidden by an anthropic cover, accumulated during centuries of urban development. This drainage network was developed mainly during the last glacial retreat (Wurmian, 18,000 years old). During this phase the urban section of the Tiber River, including its tributaries, eroded into the Plio-Pleistocene bedrock to a depth of about 50 m below the present sea level. The valleys created during this phase were subsequently filled by soft alluvial sediments in/Holocene, following the rise of the sea level since the last glacial termination (13,000 years) to the present. The recent alluvial deposits are formed by an approximately 8-m-thick basal gravel layer followed by about 50 m of poorly to nonconsolidated clay and sand sediments. These deposits are effectively always below the local level of the water table, and are characterized by poor geotechnical properties because of their weak cohesiveness and large compressibility.

By analyzing more than 1000 borehole logs, Marra and Rosa (1995) reconstructed the thickness distribution of the stratigraphic units. For zonation purposes, the geological formations can be grouped into units with approximately uniform mechanical properties (Table 2), estimated by Rovelli *et al.* (1995) from measurements for similar deposits. Information about the velocity and attenuation structure of water-saturated Holocene and Plio-Pleistocene sediments are available from Malagnini *et al.* (1995), who used explosion records from a linear array within the valley of the Chiusi Lake tributary (central Italy). The study found Q_s and V_s values ranging from 2 to 20 and 280 to 400 m/sec, respectively, for the Holocene alluvium. These Q values were used by Rovelli *et al.* (1995) for 2D simulations in the Tiber River valley. We compiled all this information into a 3D velocity model, illustrated by the individual lithological interfaces shown in Figure 3. The dimensions of the 3D model is 7.4 km by 6.6 km by 10 km deep.

Table 2
Near-Surface Viscoelastic Parameters

	ρ (kg/m^3)	V_s (m/sec)	V_p (m/sec)	Q_s	Q_p
Recent alluvium	1950	250	432	10	15
Middle Pleistocene sedimentary/volcanic deposits	1950	500	865	20	30
Pliocene clays	2000	600	1038	50	75
Carbonate	2100	1200	2076	100	150

The 3D model of Rome is included in a 1D regional model (see Fig. 4). Q_s increases from 100 near the surface to 1000 for depths greater than 30 km, whereas $Q_p = 1.5Q_s$. The elastic parameters in the transition zone between the two models are estimated by linear interpolation (100 and 50 points for the Central Apennine and Alban Hills scenarios, respectively).

Finite-Difference Modeling and Seismic Sources

We have selected two scenario earthquakes to calculate the ground motion in Rome for the two main sources of seismic hazard in Rome, namely a double-couple point source (M 5.3) in the Alban Hills and an extended fault source (M 7.0) in the Central Apennines. A fourth-order staggered-grid finite-difference method is used to calculate viscoelastic ground motion in the 3D model of Rome described in the previous section. Absorbing boundary conditions (Clayton and Engquist, 1977) are applied to the sides of the computational model. To further reduce artificial reflections the boundaries of the model are padded with a zone of attenuative material (Cerjan *et al.*, 1985). Viscoelasticity is incorporated independently for P and S waves using a coarse-grained implementation of the memory variables (Day, 1998; Day and Bradley, 2001). The seismic sources are implemented in the finite-difference grid by adding $-M_{ij}(t)/V$ to $S_{ij}(t)$, where $M_{ij}(t)$ is the ijth component of the moment tensor for the earthquake, $V = dx^3$ is the cell volume, and $S_{ij}(t)$ is the ijth component of the stress tensor on the fault at time t.

Alban Hills and Central Apennine Earthquake Scenarios

The model used for the M 5.3 Alban Hills scenario (approximately 15 km by 19 km by 10 km) was discretized into

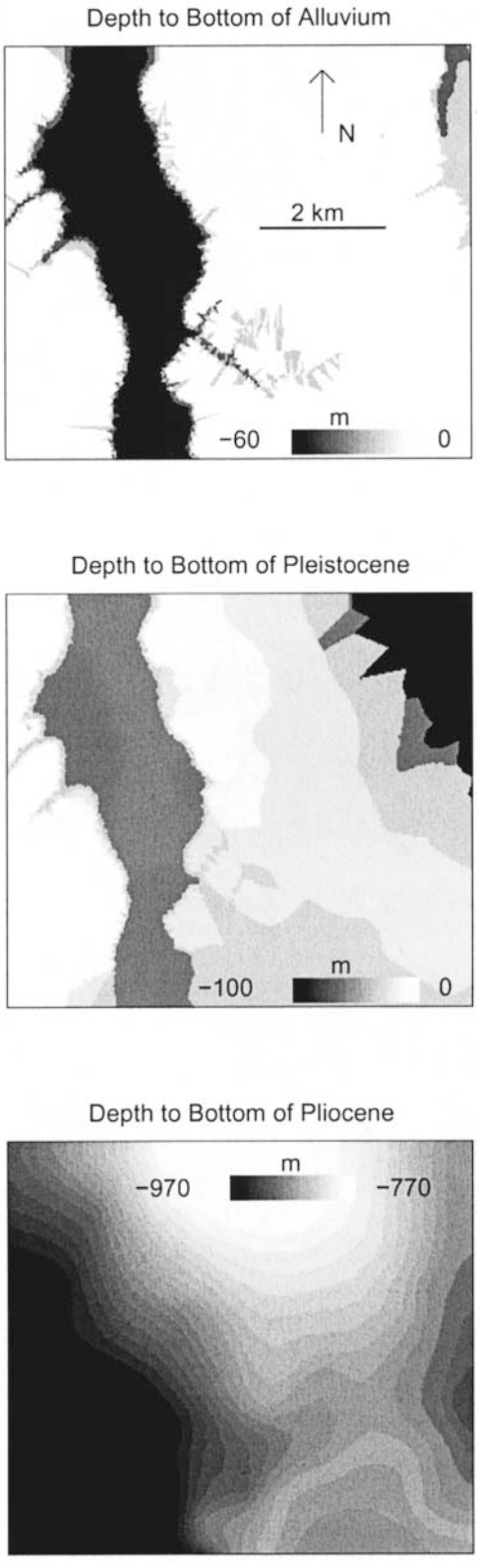

Figure 3. Lithological interfaces used to generate the 3D velocity model below Rome. (top) Depth to bottom of the alluvium. (middle) Depth to bottom of the Pleistocene. (bottom) Depth to bottom of the Pliocene.

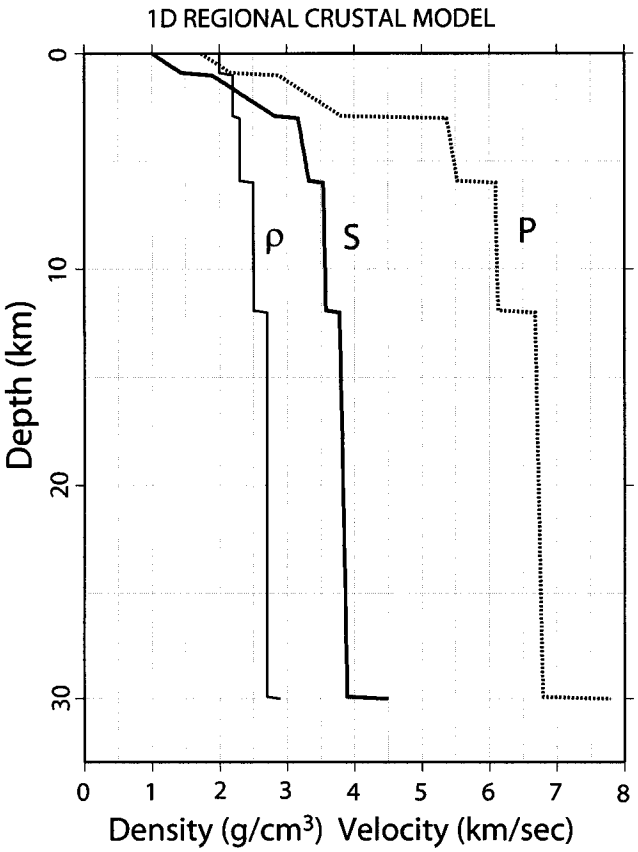

Figure 4. Regional 1D velocity and density model used in our scenario simulations.

about 24 million grid points with a grid spacing of 50 m. We used a half-cosine-shaped slip-rate function with a duration of 0.45 sec, encouraged by a good fit to data from a *M* 4.9 event for synthetics by Olsen *et al.* (2000). The Apennine scenario model had dimensions of 103 km by 29 km by 30 km, discretized into about 21 million grid points with a grid spacing of 200 m. The scenario used two variations of the six-time-window slip distribution obtained by Wald and Heaton (1994) for the 1992 Landers earthquake (mirror image of each other; see Fig. 5), for hypocentral locations toward the northwest, center, and toward the southeast of the fault (six realizations total), and a rupture velocity of 2.5 km/sec. Each time window consisted of a isosceles triangular slip-rate function with a duration of 1 sec. We used the 27.4-km-long segment of the slip model starting 10 km from the southern end of the fault (0–15 km depth). The focal depth and the source mechanism were taken from the study of Valensise and Pantosti (2001). The 3D modeling and source parameters are listed in Tables 3 and 4.

All our simulations assume at least five points per minimum shear wavelength. The Alban Hills scenario was computed using a minimum seismic velocity of 250 m/sec in the Tiber River valley sediments, limiting our analysis to ground motions less than 1 Hz. For the Central Apennine scenario computational limitations imposed a minimum velocity of

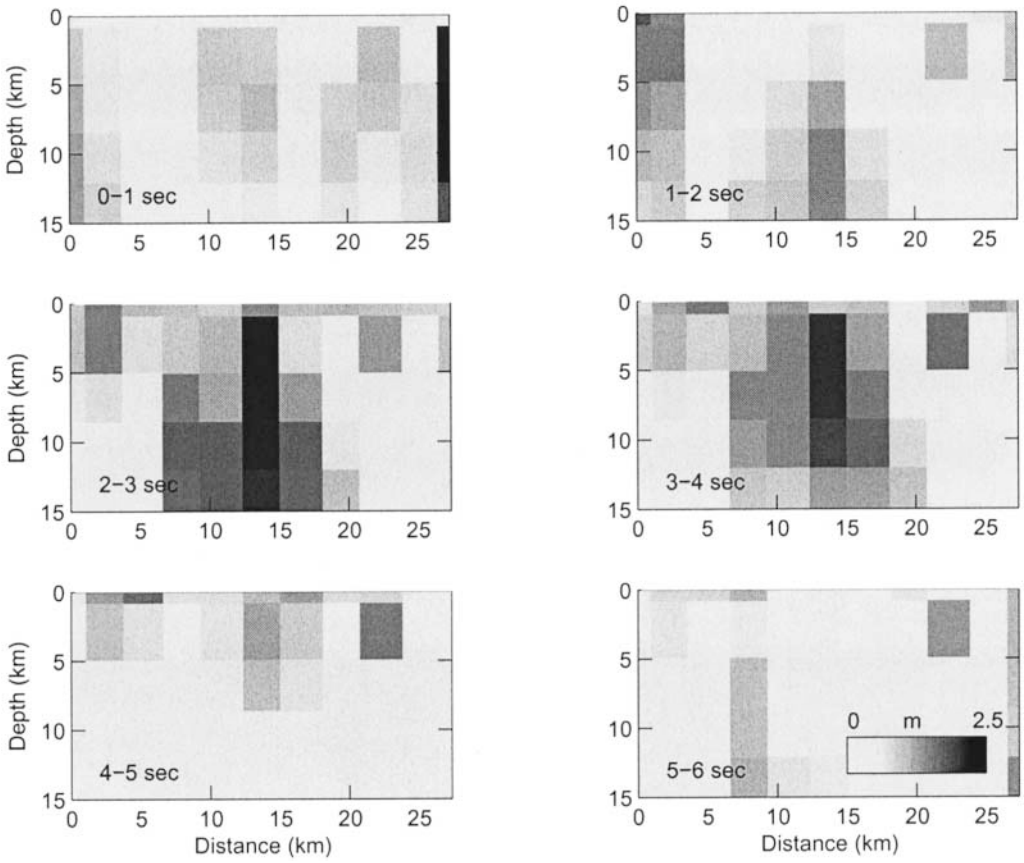

Figure 5. Six-time-window slip distribution used for the *M* 7.0 Central Apennine earthquake scenario. Two slip distributions are used: (1) shown above and (2) a lateral mirror image of (1).

Table 3
3D Modeling Parameters

Scenario	Alban Hills	Central Apennine
Spatial discretization (m)	0.05	0.20
Temporal discretization (sec)	0.004	0.012
Lowest *P*-wave velocity (m/sec)	432	865
Lowest *S*-wave velocity (m/sec)	250	500
Lowest density (kg/m^3)	1,900	1,950
Number of grid points along east–west	306	558
Number of grid points along north–south	388	207
Number of grid points along vertical	220	180
Number of time steps	10,000	12,500

Table 4
Source Parameters

Scenario	Alban Hills	Central Apennine
Strike	170°	145°
Dip	60°	60°
Rake	−45°	270°
Moment (N m)	1.010^{17}	3.5510^{19}
Depth (km)	4.4	12
Epicenter (latitude, longitude)	12.68°, 41.82°	13.49°, 42.06° (northwest) 13.60°, 41.94° (center) 13.68°, 41.85° (southeast)

500 m/sec and a maximum frequency of 0.5 Hz. However, the use of the higher minimum velocity was justified by a simulation of the Central Apennine scenario using a minimum velocity of 250 m/sec, generating a discrepancy in the 0–0.5 Hz peak velocity in Rome due to the increase in $V_s^{\min}$ of less than 5%. Moreover, because of the large distances of the Central Apennine scenario (>100 km) from Rome, the long-period approximation of the wave fields is, to a large extent, justified by a significant attenuation of the higher-frequency components of the impinging waves.

Numerical Results

In this section we use snapshots of the simulated wave propagation and peak velocity distributions to analyze the wave propagation from the Alban Hills and Central Apennines earthquake scenarios as well as a vertically incident *SH* wave within the Rome model.

Figure 6 shows snapshots of particle velocities for the Alban Hill scenario, computed for the modeled bandwidth between 0 and 1 Hz. A prominent feature in the snapshots is the criss-cross pattern of surface waves, generated at the

edges of and propagating inside the Tiber River valley. These phases are particularly apparent on the north–south component at 12.2–16.2 sec of the snapshots. These *SH*/Love waves, identified from their particle motion, are almost entirely responsible for the amplification observed within Rome. Figure 7 (top) shows the maximum peak velocities in the Tiber River valley, superimposed with the depth contours for the isosurface of $V_s = 250$ m/sec. The largest peak velocities (up to 14 cm/sec) are observed on the north–south component, in particular, along the northern boundary of the valley, amplified by basin edge effects. Figure 7 (bottom) shows synthetic seismograms from the Alban Hills scenario along the 7-km-long profile shown in Figure 7 (top), intersecting the area of the largest amplification within the model area. The synthetics clearly show the increased peak velocities above the softest sediments and, in particular, just inside the western edge of the basin.

Figure 8 shows synthetic seismograms for the Alban Hills scenario at selected locations in the center of Rome, Vatican City and the Colosseum, which are important from monumental points of view, as well as the popular Prati area (see Fig. 7 [top] for location). We find peak velocities (peak accelerations) of 2.5 cm/sec (5 cm/sec^2) in Vatican City, 2.5 cm/sec (5 cm/sec^2) at the Colosseum, both located on Quaternary deposits ($V_s = 400$ m/sec), and of 14 cm/sec (38 cm/sec^2) in the Prati area, located on the recent alluvium ($V_s = 250$ m/sec) in the middle of the Tiber River valley. The largest 1-Hz peak accelerations for the Alban Hills scenario were up to 44 cm/sec^2 in Rome.

As mentioned earlier, the largest frequency resolved in the Central Apennine scenario was 0.5 Hz because of computational limitations. For this reason, the long-period wave field impinging on the Rome area does not generate significant interaction effects with the relatively shallow valley structure. However, the peak velocities within Rome show variation due to particularly hypocentral location for the six scenarios (see Table 5). The largest peak velocities in Rome are generated by the hypocentral locations toward the southeast (9 cm/sec) and in the center (6 cm/sec), whereas hypocentral locations toward the northwest generate the smallest peak velocities (4 cm/sec). This variation is also reflected in Figure 9, showing the east–west component synthetic seismograms and peak velocities along an east–west profile from the source to Rome for the six realizations of the source. The two northwest hypocentral locations are seen to generate much weaker wave fields than the remaining scenarios, suggesting that the variation in peak motions is mainly due to source directivity effects. Notice the duration of up to 60 sec of ground motion in Rome and the slow decrease of peak velocities for about 80 km before entering Rome. This is caused by a combination of source directivity effects, surface wave generation, and a strong wave guide in the regional model, which is supported by the significant gradient in the upper 3 km of the crust shown in Figure 4. Figure 9 also shows east–west component seismograms and peak velocities for a simulation (slip "1," hypocenter "center") without anelastic attenuation. The anelastic attenuation reduces the largest horizontal peak velocities by 25%, as compared with those for the simulation with an elastic regional model, showing the importance of including a realistic Q model in the simulations.

To separate the effects of the seismic sources from the amplification pattern in Rome we have computed the ground-motion response in the city for a vertically incident planar *SH* wave, using a triangular slip-rate function with a 1-sec rise time. Figure 10 shows the 0- to 1-Hz peak velocities, relative to those obtained at a site in the Pliocene clays. The largest peak velocity amplification factor is 1.7, obtained along both sides of the valley, primarily due to basin-edge effects. This result is in agreement with the amplification effects described by the historical earthquake observations of Cifelli *et al.* (2000) and Tertulliani and Riguzzi (1995) and the numerical modeling results of Rovelli *et al.* (1995).

Table 5
Source-dependent Variation of Peak Velocities within Rome: Central Apennine Scenario

Slip Model	Hypocenter	East–West PGV (cm/sec)	North–South PGV (cm/sec)	Vertical PGV (cm/sec)
1	Center	6.1	3.2	4.3
1	Center (nq)	7.4	4.7	4.9
2	Center	6.1	3.8	4.6
1	Northwest	3.2	2.5	2.4
2	Northwest	3.5	2.4	2.6
1	Southeast	8.2	6.3	5.9
2	Southeast	9.4	5.5	6.2

nq = lossless simulation Q.

Discussion

The largest peak velocities estimated in our 3D model of Rome for the Central Apennines scenario vary from 4 cm/sec for hypocentral locations toward the northwest on the fault to 9 cm/sec for hypocentral locations in the center of the fault. These values are similar to the largest peak velocities estimated by Rovelli *et al.* (1994) (up to about 7 cm/sec). However, the durations from Rovelli *et al.* are much shorter than those obtained in our study. The main reason for this discrepancy is that Rovelli *et al.* computed the ground motions by propagating stochastically generated point-source time functions into 2D cross sections of Rome as vertically incident *SH* waves. This type of hybrid-modeling method, including that of Fäh *et al.* (1993), excludes about 100 km of wave-guide effects due to wave propagation in the crustal layers from the fault to the 3D Rome model. Figure 9 clearly shows that the train of surface waves is responsible for the longer duration estimated in the Rome area in our simulations.

Our simulations show that the strongest ground-motion amplification is restricted to the Holocene alluvial areas with

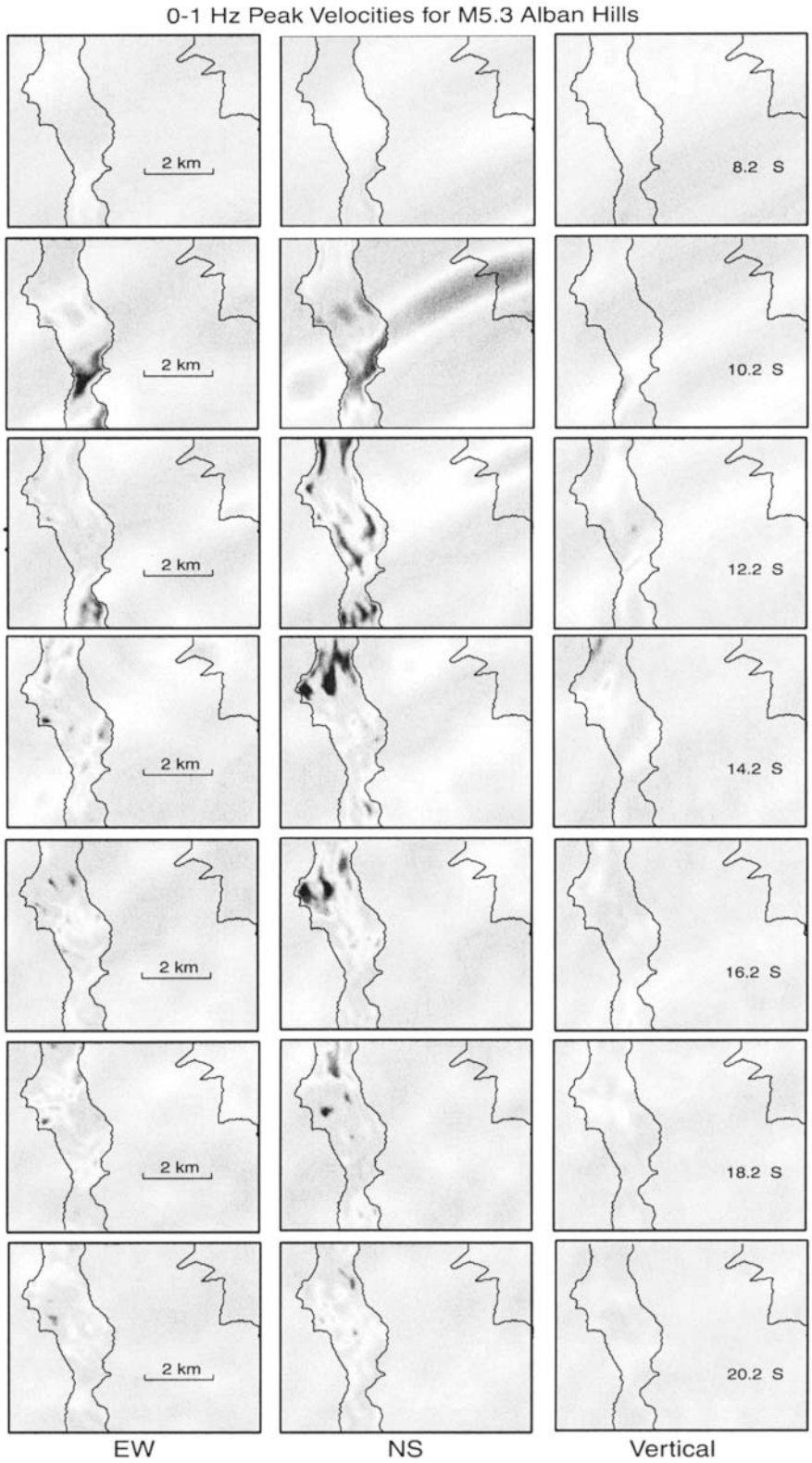

Figure 6. Snapshots of wave propagation for the M 5.3 Alban Hills scenario in Rome. The snapshots depict particle velocities at 10-sec intervals after the origin time of the earthquake. The thick line shown on the snapshots is the 50-m-depth contour of the isosurface of V_s = 250 m/sec and depicts the outline of the valley. The particle motion is scaled by the same constant for all snapshots.

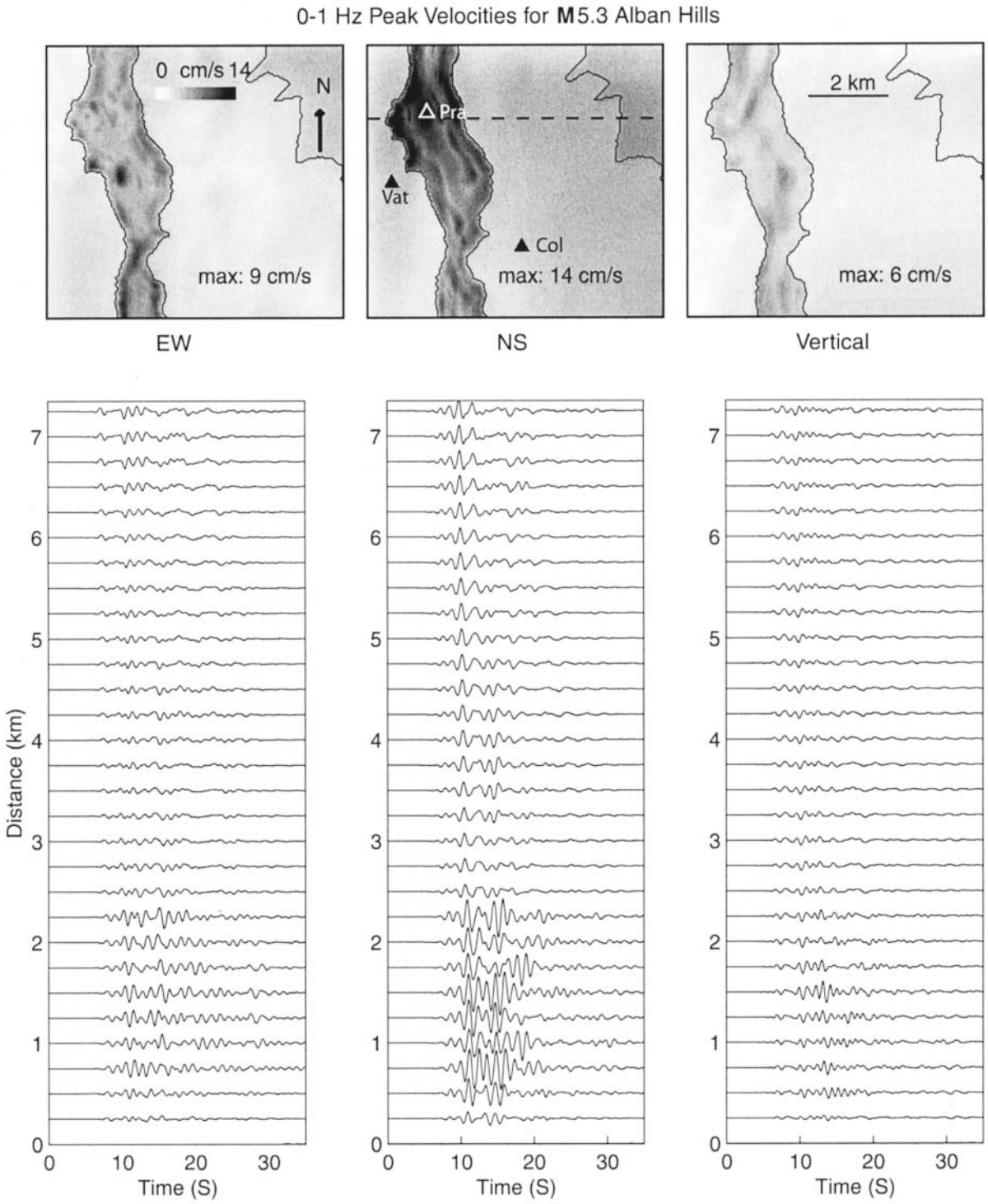

Figure 7. (top) Maps of maximum peak velocities in the Tiber River valley for the *M* 5.3 Alban Hills scenario, superimposed with the 50-m-depth contours for the isosurface of $V_s = 250$ m/sec. The peak velocities are scaled by the same constant for all components. The triangles indicate the location of Prati (Pra), Colosseum (Col), and Vatican City (Vat). The dashed line depicts the profile used to display synthetic seismograms (bottom).

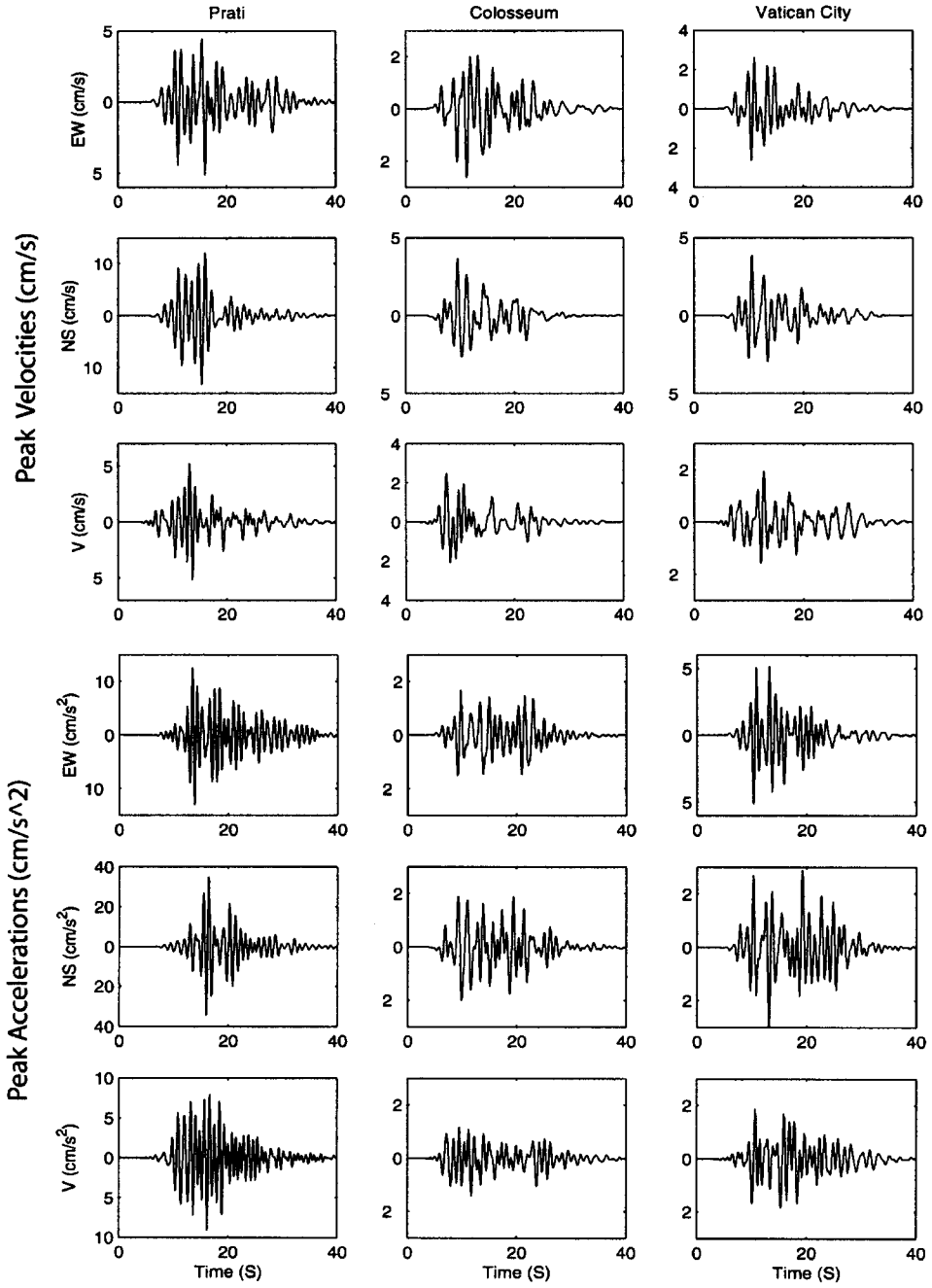

Figure 8. 3D synthetic velocities (top) and accelerations (bottom) for the Alban Hills scenario at selected locations in Rome (see Fig. 7).

a significant concentration close to the edges of the Tiber River valley. This is in agreement with the high-density macroseismic survey results of Cifelli *et al.* (2000) which were obtained after both the 14 October 1997 (M_w 5.6) and the 26 March 1998 (M_w 5.3) Umbria-Marche earthquakes. They correlated the intensity data for the two earthquakes with the local geology within the modern urban area of Rome. They observed that, on average, the alluvial deposits, in particular, near the edges of the valley, were prone to higher intensity by one MCS degree with respect to volcanic and sedimentary bedrock formations, in agreement with our results from the Alban Hills scenario simulation. Furthermore, our estimate of amplification values up to 1.7 for a vertically incident plane *SH* wave is in agreement with the value of 1.5 from the 2D simulations by Rovelli *et al.* (1994). Finally, the occurrence of the strongest earthquake damage in the city also seems to be restricted to the Holocene sediments, as documented by a macroseismic survey of damage in Rome by earthquakes from the twentieth century (Molin *et al.*, 1995).

Conclusions

We have generated a 3D velocity model for Rome, Italy, and used the model to compute long-period ground motions

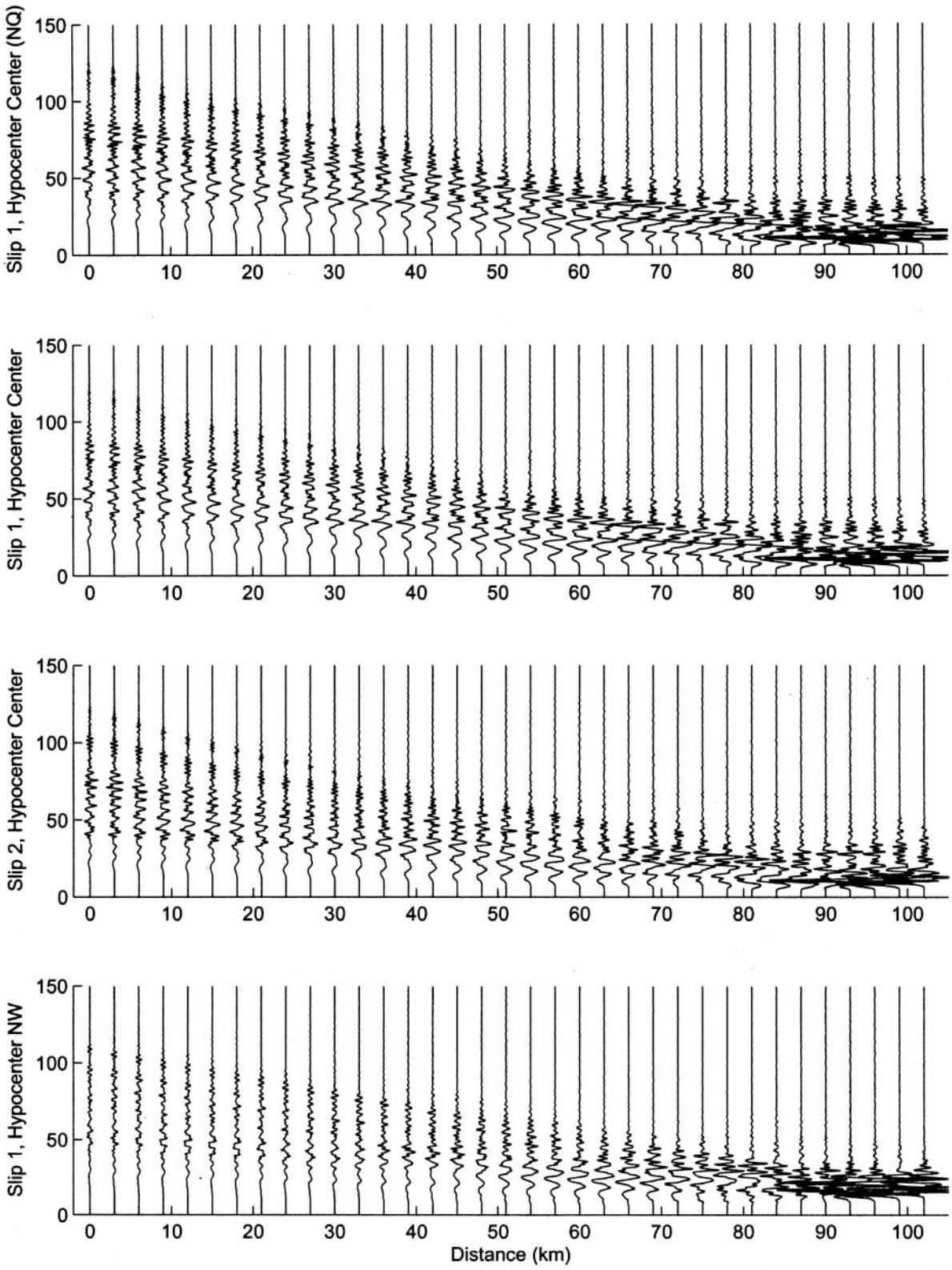

Figure 9. East–west component seismograms along an east–west profile from the fault to Rome for the *M* 7.0 Apennine scenario earthquake, for six different realizations of the source process (hypocentral location toward the northwest, center, and southeast of the fault, and slip distributions 1 and 2, see Fig. 5) and their east–west peak velocities (bottom). The top panel shows the east–west seismograms for a simulation with an elastic (loss-less) regional model and hypocenter location in the center of the fault and slip distribution 1. (*continued*)

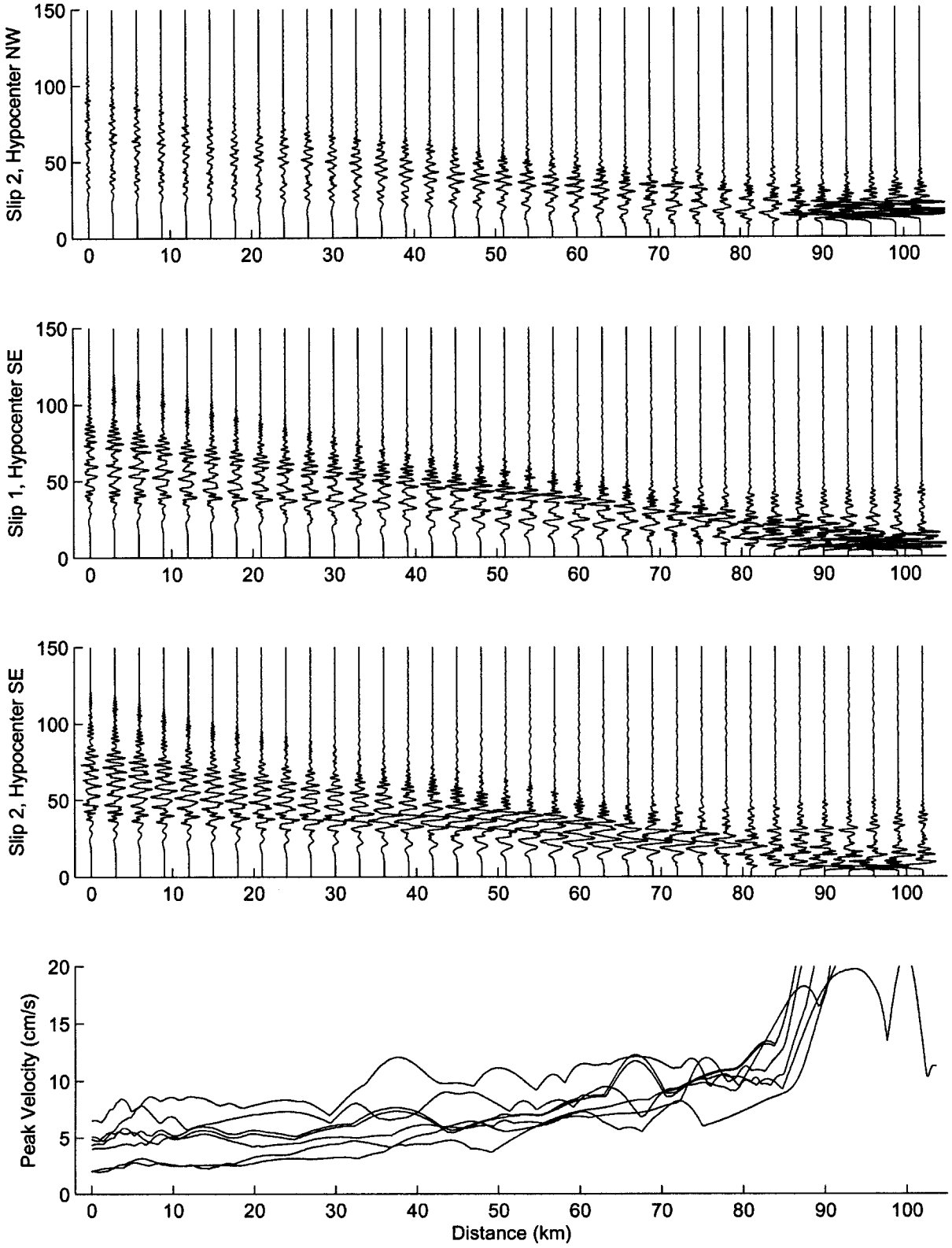

Figure 9. Continued.

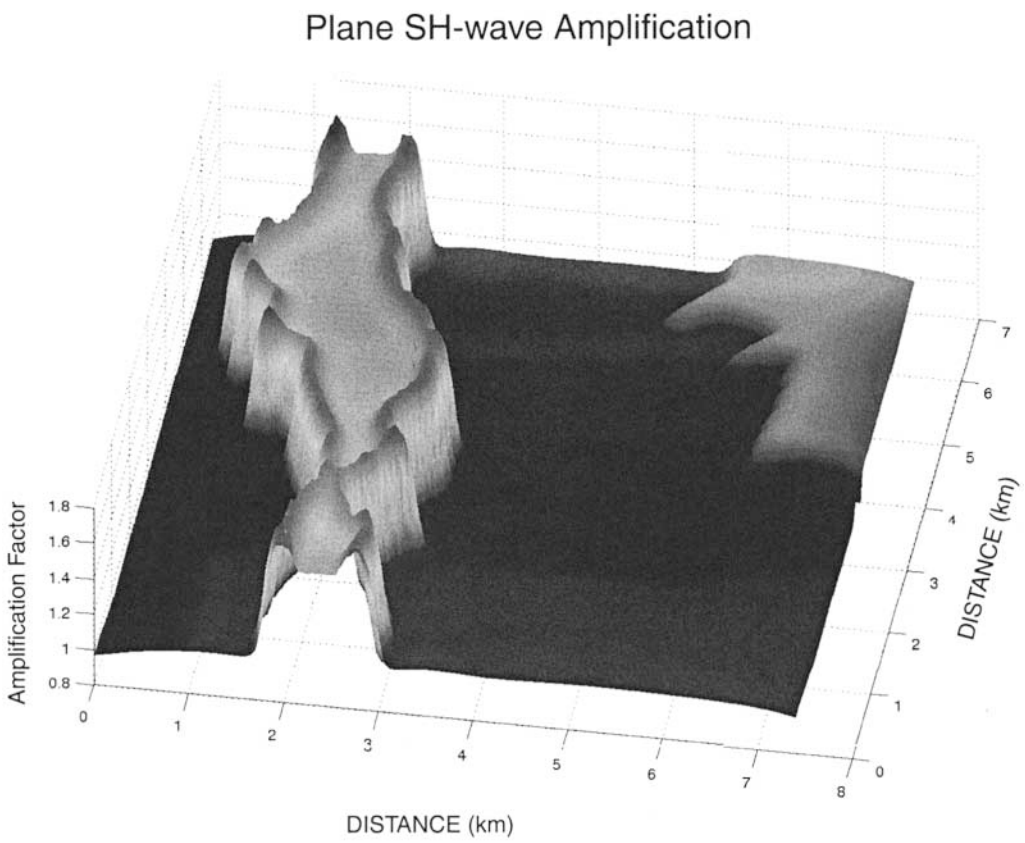

Figure 10. 0–1 Hz peak velocities in Rome, relative to the value in rock, for a vertically incident planar *SH* wave.

for two credible earthquake scenarios in the vicinity of Rome (*M* 5.3 from Alban Hills, about 25 km to the southeast, and *M* 7 from central Apennines, about 100 km to the east). The simulations show that the strongest ground-motion amplification is restricted to the Holocene alluvial areas with a significant concentration close to the edges of the Tiber River valley. We find 0 to 1-Hz peak ground velocities and accelerations of up to 14 cm/sec and 44 cm/sec^2, respectively, for the Alban Hills earthquake, largest near the northwestern edges of the Tiber River because of focusing effects and surface-wave generation. For the Central Apennine earthquake we estimate a maximum 0 to 0.5-Hz peak velocity of 9 cm/sec with an extended duration of about 60 sec, due to source directivity, large-surface-wave generation, and crustal wave-guide effects. This result is important because the historic buildings of Rome are likely weakened to an extent that may not be able to withstand such duration of ground motions. Simulation with a vertically incident *SH*-wave source shows that the fill deposits in the Tiber River amplify the ground motion by up a factor of 1.7 with respect to the surrounding volcanic formations.

This study is a first step toward 3D physics-based prediction of seismic hazards in the Tiber River valley of Rome for a future large earthquake and more accurate probabilistic seismic-hazard analysis. Future work should extend these results to include higher-frequency ground motions, either by higher-resolution numerical models or a combination of low-frequency (3D) numerical synthetics and high-frequency (stochastic) synthetics.

Acknowledgments

We are grateful to Andrea Bono for digitizing the 3D map of the Tiber River valley. SDSU, INGV, and Group CED provided CPU time on SUN and NEC-4 computers for our 3D simulations. We thank A. Tertulliani and A. Caserta for their helpful reviews of the manuscript. The study was supported by the Institute for Geophysics and Planetary Physics (IGPP) (to K.B.O.) and the Istituto Nazionale di Geofisica e Vulcanologia, Rome (to A.A., A.R., F.M., L.M.).

References

Amato, A., C. Chiarabba, M. Cocco, M. Di Bona, and G. Selvaggi (1994). The 1989–1990 seismic swarm in the Alban Hills volcanic area, central Italy, *J. Volcanol. Geotherm. Res.* **61,** 225–237.

Ambrosini, S., S. Castenetto, F. Cevolan, E. Di Loreto, R. Funiciello, L. Liperi, and D. Molin (1986). Risposta sismica dell'area urbana di Roma in occasione del terremoto del Fucino del 13-1-1915, *Mem. Soc. Geol. Ital.* **35,** 445–452.

Basili, A., L. Cantore, M. Cocco, A. Frepoli, L. Margheriti, C. Nostro, and G. Selvaggi (1996). The June 12, 1995 microearthquake sequence in the City of Rome, *Ann. Geofis.* **39,** no. 6, 1167–1175.

Boschi, E., A. Caserta, C. Conti, M. Di Bona, R. Funiciello, L. Malagnini, F. Marra, G. Martines, A. Rovelli, and S. Salvi (1995). Resonance of subsurface sediments: an unforeseen complication for designers of roman columns, *Bull. Seism. Soc. Am.* **85,** no. 1, 320–324.

Cerjan, C., D. Kosloff, R. Kosloff, and M. Reshef (1985). A nonreflecting boundary condition for discrete acoustic and elastic wave equations, *Geophysics* **50,** 705–708.

Chiarabba, C., L. Malagnini, and A. Amato (1994). Three-dimensional velocity structure and earthquake relocation in the Alban Hill volcano, central Italy, *Bull. Seism. Soc. Am.* **84,** 295–306.

Cifelli, F., S. Donati, F. Funiciello, and A. Tertulliani (2000). High-density macroseismic survey in urban areas, part 2: results for the city of Rome, Italy, *Bull. Seism. Soc. Am.* **90,** no. 2, 298–311.

Clayton, R., and B. Engquist (1977). Absorbing boundary conditions for acoustic and elastic wave equations, *Bull. Seism. Soc. Am.* **71,** 1529–1540.

Day, S. (1998). Efficient simulation of constant Q using coarse-grained memory variables, *Bull. Seism. Soc. Am.* **88,** 1051–1062.

Day, S. M., and C. Bradley (2000). Memory-efficient simulation of anelastic wave propagation, *Bull. Seism. Soc. Am.* **91,** 520–531.

Donati, S., R. Funiciello, and A. Rovelli (1999). Seismic response in archaeological areas: the case histories of Rome, *J. Appl. Geophys.* **41,** 229–239.

Fäh, D., C. Iodice, P. Suhaldoc, and G. Panza (1993). A new method for the realistic estimation of seismic ground motion in megacities: the case of Rome, *Earthquake Spectra* **9,** 643–667.

Fäh, D., C. Iodice, P. Suhaldoc, and G. Panza (1995). Application of numerical simulations for a tentative seismic microzonation of the city of Rome, *Ann. Geofis.* **38,** no. 5–6, 607–616.

Frankel, A., and J. Vidale (1992). A three-dimensional simulation of seismic waves in the Santa Clara Valley, California, from a Loma Prieta aftershock, *Bull. Seism. Soc. Am.* **82,** 2045–2074.

Funiciello, R., L. Lombardi, F. Marra, and M. Parotto (1995). Seismic damage and geological heterogeneity in Rome's Colosseum area: are they related? *Ann. Geofis.* **38,** no. 5-6, 927–938.

Graves, R. (1996). Simulating seismic wave propagation in 3D media using staggered-grid finite differences, *Bull. Seism. Soc. Am.* **86,** 1091–1106.

Gruppo di Lavoro CPTI (1999). Catalogo Parametrico dei Terremoti Italiani, Instituto Nazionale di Geofisica (ING), Gruppo Nazionale par la Difesa dai Terremoti (GNDT), Storia Geofisica e Ambiente (SGA), Servizio Sismico Nazionale (SSN), Bologna, 92 pp.

Hadjian, A. H. (1993). The Spitak, Armenia earthquake of 7 December 1988—Why so much destruction? *Soil Dyn. Earthquake Eng.* **12,** 1–24.

Iodice, C., D. Fäh, P. Suhadolc, and G. F. Panza (1992). Un metodo generale per la zonazione sismica immediata ed accurata di grandi metropoli: applicazione alla citta di Roma, *Rend. Fis. Acc. Lincei*, **9,** no. 3, 195–217.

Kawase, H. (1996). The cause of the damage belt in Kobe: the basin-edge effect, constructive interference of the direct S-wave with the basin-induced diffracted/Rayleigh waves, *Seism. Res. Lett.* **67,** 25–34.

Malagnini, L., R. B. Herrmann, G. Biella, and R. de Franco (1995). Rayleigh waves in Quaternary alluvium from explosive sources: determination of shear-wave velocity and Q structure, *Bull. Seism. Soc. Am.* **85,** 900–922.

Marra, F., and C. Rosa (1995). Stratigrafia e assetto geologico dell'area romana, in *Mem. Descr. Carta Geol. Ital. La Geologia di Roma. Il Centro Storico* **50,** 49–118.

Molin, D., and E. Guidoboni (1989). Effetto fonti effetto monumenti a Roma: i terremoti dall 'antichità ad oggi, in l terremoti prima del Mille in Italia e nell' Area Mediterranea, E. Guidoboni (Editor), ING, Bologna, 194–223 (in Italian).

Molin, D., S. Castenetto, E. Di Loreto, E. Guidoboni, L. Liperi, B. Narcisi, A. Paciello, F. Riguzzi, A. Rossi, A. Tertulliani, and G. Traina (1995). Sismicità, in *Mem. Descr. a Carta Geol. Ital. La Geologia di Roma Il centro storico*, R. Funiciello (Editor), **50,** 323–408.

Motosaka, M., and M. Nagano (1997). Analysis of amplification characteristics of ground motions in the heavily damaged belt zone during the 1995 Hyogoken-Nanbu earthquake, *Earthquake Eng. Struct. Dyn.* **26,** no. 3, 877–395.

Olsen, K. B. (2000). Site amplification in the Los Angeles Basin from 3D modeling of ground motion, *Bull. Seism. Soc. Am.* **90,** S77–S94.

Olsen, K. B., and R. J. Archuleta (1996). Three-dimensional simulation of earthquakes on the Los Angeles Fault System, *Bull. Seism. Soc. Am.* **86,** 575–596.

Olsen, K. B., and G. T. Schuster (1995). Causes of low-frequency ground motion amplification in the Salt Lake Basin: The case of the vertically-incident P wave, *Geophys. J. Int.* **122,** 1045–1061.

Olsen, K. B., S. M. Day, and C. R. Bradley (2003). Estimation of Q for long-period (>2 s) waves in the Los Angeles Basin, *Bull. Seism. Soc. Am.* **93,** 627–638.

Olsen, K. B., J. C. Pechmann, and G. T. Schuster (1995). Simulation of 3-D elastic wave propagation in the Salt Lake Basin, *Bull. Seism. Soc. Am.* **85,** 1688–1710.

Pantosti, D., G. D'Addezio, and F. R. Cinti (1996). Paleoseismicity of the Ovindoli-Pezza fault (Central Italy): a history including a large, previously unrecorded earthquake in Middle Ages (886–1300 A.D.), *J. Geophys. Res.* **X,** 5937–5959.

Pitarka, A., K. Irikura, T. Iwata, and T. Kagawa (1996). Basin structure effects in the Kobe area inferred from the modeling of ground motions from two aftershocks of the January 17, 1995, Hyogoken-nanbu earthquake, *J. Phys. Earth* **44,** 563–576.

Rovelli, A., A. Caserta, L. Malagnini, and F. Marra (1994). Assessment of potential strong ground motion in the city of Rome, *Ann. Geofis.* **37,** no. 6, 1745–1769.

Rovelli, A., L. Malagnini, A. Caserta, and F. Marra (1995). Using 1-D and 2-D modelling of ground motion for seismic zonation criteria: results for the city of Rome, *Ann. Geofis.* **38,** no. 5-6, 591–605.

Salvi, S., E. Boschi, M. Di Bona, R. Funiciello, L. Malagnini, F. Marra, and A. Rovelli (1991). Subsurface geology and variations of seismic response in the city of Rome, in *Fourth International Conference on Seismic Zonation,* Stanford, California, 26–28 August 1991, 115–122.

Seekins, L. C., and L. C. Boatwright (1994). Ground motion amplification, geology, and damage from the 1989 Loma Prieta earthquake in the city of San Francisco, *Bull. Seism. Soc. Am.* **84,** 16–30.

Sieberg, A. (1930). Geologie der Erdbeben, *Handb. Geophys.* **2,** no. 4, 550–555.

Singh, S. K., E. Mena, and R. Castro (1988). Some aspects of source characteristics of the 19 September 1985 Michoacan earthquake, and ground motion amplification in and near Mexico City from strong motion data, *Bull. Seism. Soc. Am.* **78,** 451–477.

Tertulliani, A., and F. Riguzzi (1995). Earthquakes in Rome during the past one hundred years, *Ann. Geofis.* **38,** no. 5-6, 581–590.

Valensise, G., and D. Pantosti (Editors) (2001). Database of potential sources for earthquakes larger than M 5.5 in Italy, *Ann. Geofis.* **44** (Suppl. 1), with CD-Rom.

Wald, D. J., and R. W. Graves (1998). The seismic response of the Los Angeles Basin, California, *Bull. Seism. Soc. Am.* **88,** 337–356.

Wald, D. J., and T. Heaton (1994). Spatial and temporal distribution of slip for the 1992 Landers, California, earthquake, *Bull. Seism. Soc. Am.* **84,** 668–691.

Yomogida, K., and J. T. Etgen (1993). 3-D wave propagation in the Los Angeles basin for the Whittier Narrows earthquake, *Bull. Seism. Soc. Am.* **83,** 1325–1344.

Department of Geological Sciences
5500 Campanile Drive
San Diego State University
San Diego, California 92182-1020
(K.B.O.)

Istituto Nazionale di Geofisica e Vulcanologia
Via di Vigna Murata
605 00143 Rome, Italy
(A.A., A.R., F.M., L.M.)

Manuscript received 8 December 2003.